Euro PM2019 – Powders for AM - Recycling

Manuscript refereed by Dr Riccardo Casati (Politecnico di Milano, Italy)

Automated SEM/EDS Analysis for Assessment of Contamination and Non-Metallic Inclusions of Powders and Additive Manufactured Inconel 718 Alloy

Maria J. Balart[1*], Xinjiang Hao[1,2] Samuel Marks[1], Geoff D. West[1] Claire L. Davis[1]
[1]University of Warwick, WMG – Advanced Manufacturing and Materials Centre (AMMC), Coventry CV4 7AL, UK
[2]Liberty Speciality Steels, 7 Fox Valley Way, Stocksbridge, Sheffield S36 2JA, UK
*Corresponding author email: M.Balart-Murria@warwick.ac.uk
Xinjiang.Hao@libertypowdermetals.com G.West@warwick.ac.uk; Claire.Davis@warwick.ac.uk

Abstract:
Inconel 718 alloy can consistently be additive manufactured. However, cross-contamination of the powder precursors can occur during powder production, handling and additive manufacturing. The use of automated SEM/EDX is reported to assess contamination and non-metallic inclusions along with the corresponding microstructures in the powders and additive manufactured IN718 alloy product which was heat-treated as per AMS5662.

Introduction

IN718 can consistently be additive manufactured [1]. Powder precursors from IN718 can be produced by plasma atomisation to a high surface purity, however, the surfaces can be degraded by the formation of sub-micron sized particulate oxide features after being subjected to up to four cycles of powder recycling during additive manufacturing (AM), for example during AM by electron beam melting (EBM) [2]. Although, the type of sub-micron sized particles in the four times recycled IN718 powder were not reported in Ref. [2], the authors showed fine Cr-Al rich oxide particulates (20 nm approx.) on the surface of Ni-based superalloy Hastelloy X powder recycling after laser sintering (LS) processing. Compared with wrought product (e.g. grades AMS5662 [3] and AMS5383 [4]) [5], selective laser melting (SLM) products subjected to both solution and aging (SA) as well as homogenisation + solution + aging (HSA) standard heat treatments have been reported to exhibit slightly superior strength levels at room temperature (RT), i.e. 1046-1084 MPa c.f. 1034 MPa YS and 1371 MPa c.f. 1276 MPa UTS. The ductility of the SA condition, however, is slightly lower (10.1% c.f. 12.0% El. at RT) and that of the HAS condition is similar (12.3% El c.f. 12.0% El. at RT). Precipitation strengthening in the γ Cr-Ni matrix was achieved by nm-sized $L1_2$-ordered γ' Ni_3(Al,Ti) fcc phase and $D0_{22}$-ordered γ'' Ni_3[Nb,Ti,Al] bct phase but μm-sized δ phase was observed (more in the SA condition than in the HSA condition). No δ phase was reported in the as-built product [5], only after heat treatment; it was predicted, using DICTRA simulations, that the onset for δ precipitation could occur at 30 h, for IN625 wrought alloy composition, whilst at 1 min. when the local change in Nb composition exceed the upper limit for the IN626 specification [6], which can occur due to segregation in the powder. On the other hand, mainly Laves phases and MC-type carbides were found in the as-fabricated condition [5]. Despite the presence of δ phase in the SLM + STA material a similar combination of strength and ductility levels were achieved compared with those of wrought + STA product (1271 and 1216 MPa YS, 1425 and 1425 MPa UTS and 18.6 and 24.0% El., respectively) at RT and (1042 and 1028 MPa YS and 1142 and 1139 MPa UTS and 10.1 and 10.5% El., respectively) at 650^{o}C [7], noting the higher values of strength and ductility compared to that reported by Zhang *et al.* [5]. However, it has been reported that δ phase embrittlement can occur for tensile and creep testing at 650^{o}C in HIP'd IN718 followed by solution and aging heat treatments [7].

Besides possible cross-contamination of powder precursors during powder production, handling and AM [8-10], discrete sub-micron sized oxide particles can form at powder surfaces during AM processing by LS and EBM [2] and spatter in laser powder bed fusion of IN718 alloy [11]. This paper focuses on the assessment of contamination and non-metallic inclusions in powders and additive manufactured Inconel 718 alloy by using automated SEM/EDX [12,13] to consider the size, number and distribution of contaminants; in addition the corresponding microstructures will also be discussed briefly for analysis and to provide comparison with previously published cases.

Experimental

AM samples using SLM with a Renishaw AM 250 from vacuum induction gas atomized (VIGA) Ni-based superalloy IN718 powders (sieved to 25 - 63 μm) were supplied via Liberty Speciality Steels. The AM

samples were heat treated to SA as laid down in Standard AMS 5662: solution treatment 980°C for 1 h, air-cooling, double aging at 720°C for 8 h, furnace cooled to 620°C and then held isothermally for 8 h before final air-cooling. The chemical compositions of the alloy powder and AM sample investigated are given in Table 1. The C and S contents of the samples were determined using an Eltra™ CS-2000 carbon/sulphur analyser equipped with a high-frequency induction furnace. The N and O content of the samples were analysed by LECO™. The other elements were analysed by inductively coupled plasma optical emission spectrometry (ICP-OES).

Table 1. Chemical composition (wt.%) of the investigated IN718 alloy powders and AM+SA samples.

Alloy		B	Co	Cr	Cu	Mn	Mo	Ni	P	Si	Mg	Fe
AMS 5662	min.			17			2.80	50				Bal.
	max.	0.006	1	21	0.30	0.35	3.30	55	0.0015	0.35		
25 – 63 µm		0.0002	0.102	19.4		0.0104	3.03	52.2	0.0002	0.0663	0.0009	
AM+SA		<0.0050	0.260	18.86	<0.02	<0.02	2.99	53.69	<0.005	0.02		17.45

Alloy		Ta	Al	Ti	Nb	Pb	Bi	Se	C	S	N	O
AMS 5662	min.		0.20	0.65	4.75							
	max.	0.05	0.80	1.15	5.50	0.0005	0.00003	0.0003	0.08	0.015		
25 – 63 µm		0.0034	0.480	0.964	4.99				0.0419	0.00305	0.0150	0.0140
AM+SA		<0.02	0.480	0.93	4.98	<0.0050	<0.0050	<0.0050	0.04	0.003	0.0180	0.0270

An XRD pattern from the IN718 powder (sieved to 25 - 63 µm) was recorded by using a Panalytical Empyrean (Iona) X-ray diffractometer with Co *Kα* radiation ($\lambda_{K\alpha1}$ = 0.178901 nm, $\lambda_{K\alpha2}$ = 0.17929 nm, $I_{K\alpha2}$ / $I_{K\alpha1}$ = 0.5 at a voltage of 40 kV and a current of 40 mA. The X-ray diffraction measurements were carried out within the scan range of 40°-70° 2θ with step size of 0.000744 2θ. The spectra were indexed and identified using the HighScore Plus software and the Joint Committee on Powder Diffraction Standards (JCPDS) International Centre for Diffraction Data [14].

SEM backscattered electron imaging (BSEIing) and EDS were carried out using a Zeiss Sigma FEG-SEM and a Versa 3D dual beam SEMs operating at 10 kV. Elemental analyses and mappings were processed using the Aztec OI software feature that integrates EDS analysis software with an XMax 50 SDD (Silicon Drift Detector) and an XMax 80 SDD, respectively. BSEIs in conjunction with EDS in the Versa SEM were used to assess contamination and to quantify the size (maximum dimension) and number density of inclusions on polished powders following cold mounting and Au sputtering. AM+SA samples were examined in the SEM on a polished section for inclusion analysis and fractographically for Charpy V-notch impact specimens tested at room temperature.

Results and Discussion

Fig. 1 shows a cross-contamination particle (Al-rich), which was found in the gas-atomised IN718 powder and also confirmed in a parallel assessment [10]. The foreign Al-based contaminant has been classified as type VI in the contamination classification system proposed by MTC [9] and is of an unknown source. The area of such particle was 395 µm^2 corresponding to an area fraction of 9.78 x 10^{-5}, from a total scanned area of 4.04 mm^2. Santecchia *et al.* [8] reported average calculated cross-contamination values in the range of (1.8 ± 0.5) 10^{-3} and (7 ± 1) 10^{-3} in deliberately contaminated powders by using BSEIing in conjunction with EDS on powders sprinkled on SEM stubs from five micrographs at x500 magnification and extrapolated to a stub area of 122.6 mm^2 (repeated three times for each cross-contamination condition). In light of this, the authors propose SEM/EDS in conjunction with statistical data analyses for quality control of raw materials introduced in the supply chain to future standarisation as very small amounts of contamination can be identified. Examination of powder surfaces, Fig. 2, revealed micron-sized and thermally stable Al-Ti-(Mg) oxides on the surface. BSEI and EDS of powder cross-sections identified an Al-Ti-(Mg) oxide inclusion (S1), matrix (S2) and

microsegragation (S3), Fig. 3. Hryha *et al.* [2] reported finer surface particulates in both alloy 718 recycled powder after four cycles of EBM processing and Hastealloy X powder after one LS cycle from powder precursors produced by plasma atomization and VIGA, respectively. On the other hand, Gasper *et al.* [11] reported coarser spatter particles in laser powder bed fusion IN718. XRD analysis for the Inconel 718 alloy powder, as-built AM and AM+SA samples are shown in Fig. 4 from where it can be seen (i) γ'' $NbNi_3$ phase (bct, space group I4/mmm, 3.6200 Å, 3.6200 Å, 7.4100 Å) overlapping with γ Cr-Ni matrix (fcc, space group Fm-3m, 3.5910 Å); (ii) the presence of δ $NbNi_3$ phase

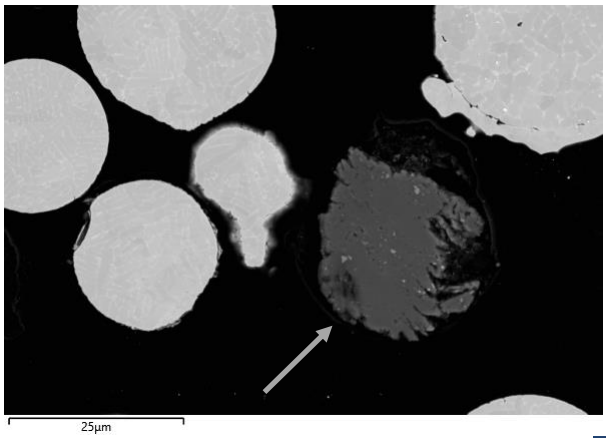

Figure 1. BSE micrograph for IN718 alloy powder showing an irregular foreign Al-based material (arrowed). Area of analysis: 59 x 85.9 x 10^{-6} mm^2 size of field, 1864 number of fields, 5.41 mm^2 area of resin and 4.04 mm^2 area scanned.

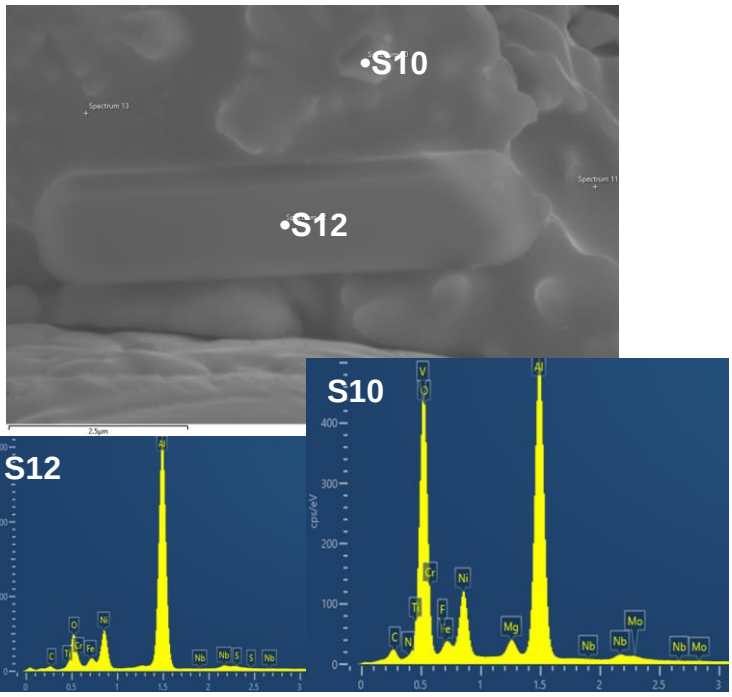

Figure 2. BSE micrographs and EDS analysis of gas-atomised IN718 powder showing cluster particulates on the powder surface.

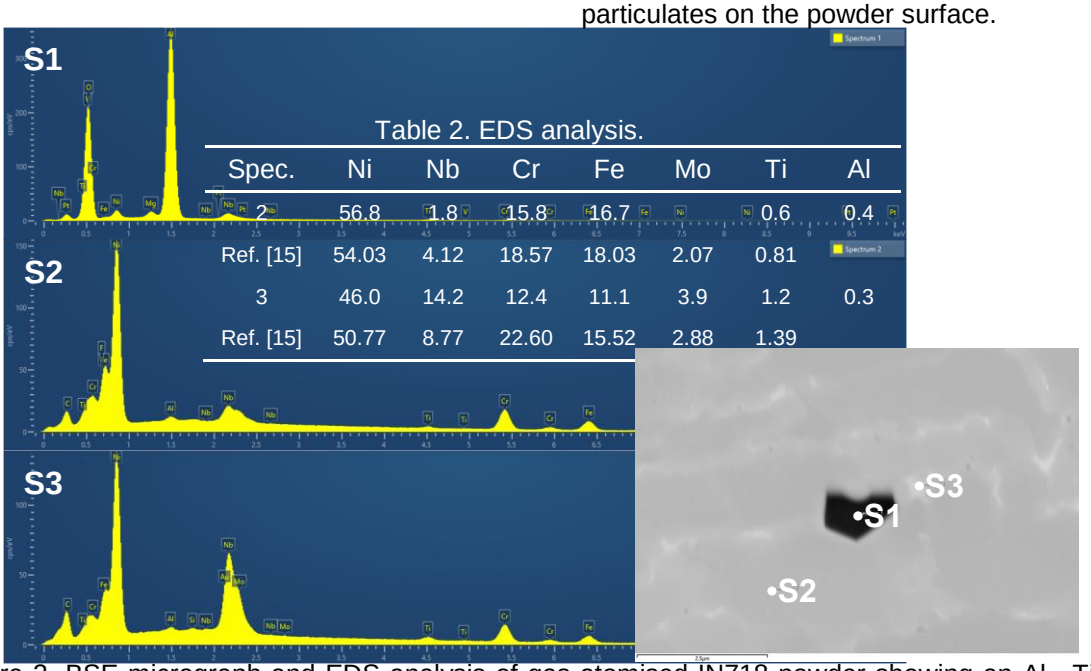

Table 2. EDS analysis.

Spec.	Ni	Nb	Cr	Fe	Mo	Ti	Al
2	56.8	1.8	15.8	16.7		0.6	0.4
Ref. [15]	54.03	4.12	18.57	18.03	2.07	0.81	
3	46.0	14.2	12.4	11.1	3.9	1.2	0.3
Ref. [15]	50.77	8.77	22.60	15.52	2.88	1.39	

Figure 3. BSE micrograph and EDS analysis of gas-atomised IN718 powder showing an Al-, Ti- and Mg-rich inclusion (S1) and a Nb-, Mo-, Ti- and C-rich microsegregation region that is Cr- and Ni-depleted (S3) compared to the matrix (S2). Area of analysis: 59 x 85.9 x 10^{-6} mm^2 size of field, 1864 number of fields, 5.41 mm^2 area of resin and 4.04 mm^2 area scanned. EDS analysis from dendrites (grey phase) and interdendritic areas (white phase) from Ref. [15] have also been included for comparison.

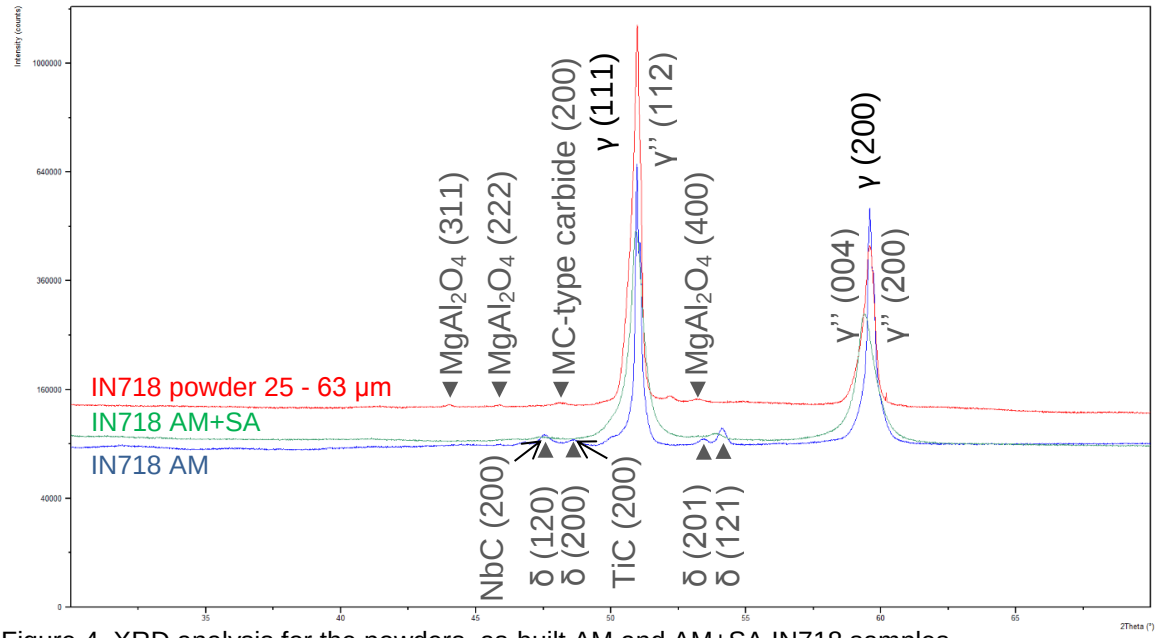

Figure 4. XRD analysis for the powders, as-built AM and AM+SA IN718 samples.

(orthorhombic, space group Pmmn, 4.5650 Å, 5.1160 Å, 4.2600 Å) in the as-built AM and AM+SA samples; (iii) (200) peaks of MC-type carbides: TiC (fcc, space group Fm-3m, 4.3300 Å) and NbC (fcc, space group Fm-3m, 4.4698 Å) and (iv) a small peak appearing at the peak positions for (311), (222) and (400) inherent to $MgAl_2O_4$ (fcc, space group Fd-3m, 8.0860 Å) in the powder sample Fig. 4.

Automated SEM images of the inclusions was performed on an AM+SA sample Figs. 5, and the corresponding histograms of number density of inclusions are shown in Fig. 6, from which it can be seen that they are predominantly Al-Ti-(Mg) oxides, Mg being a residual element. Mapping of elements from precipitates in AM+SA IN718 is shown in Fig. 7. Whilst micron-sized Al_2O_3 particles (S12) and Al-TI oxide particles (S10) formed larger clusters on the powder surface (Fig. 2), larger single globular, irregular and elliptically elongated Al-Ti oxide particles were observed in the AM+SA sample (Fig. 5).

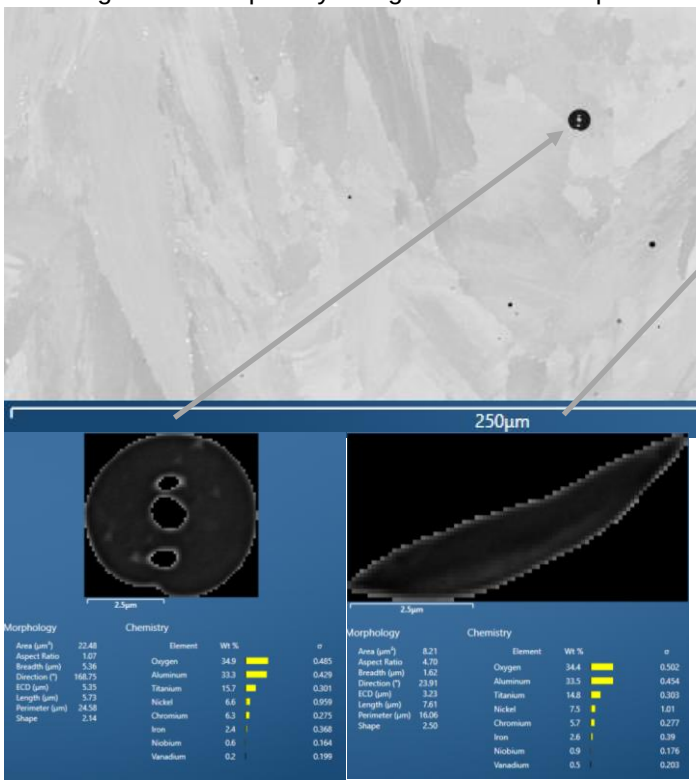

Figure 5. Inclusions maps for the AM+SA IN718 sample. Area of analysis: 59 x 85.9 x 10^{-6} mm^2 size of field, 1320 number of fields and 6.69 mm^2 area scanned.

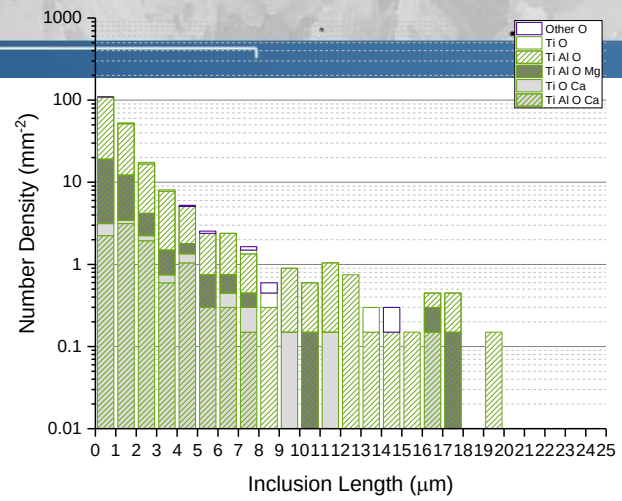

Figure 6. Histogram of number density of inclusions in additive manufactured IN718 alloy.

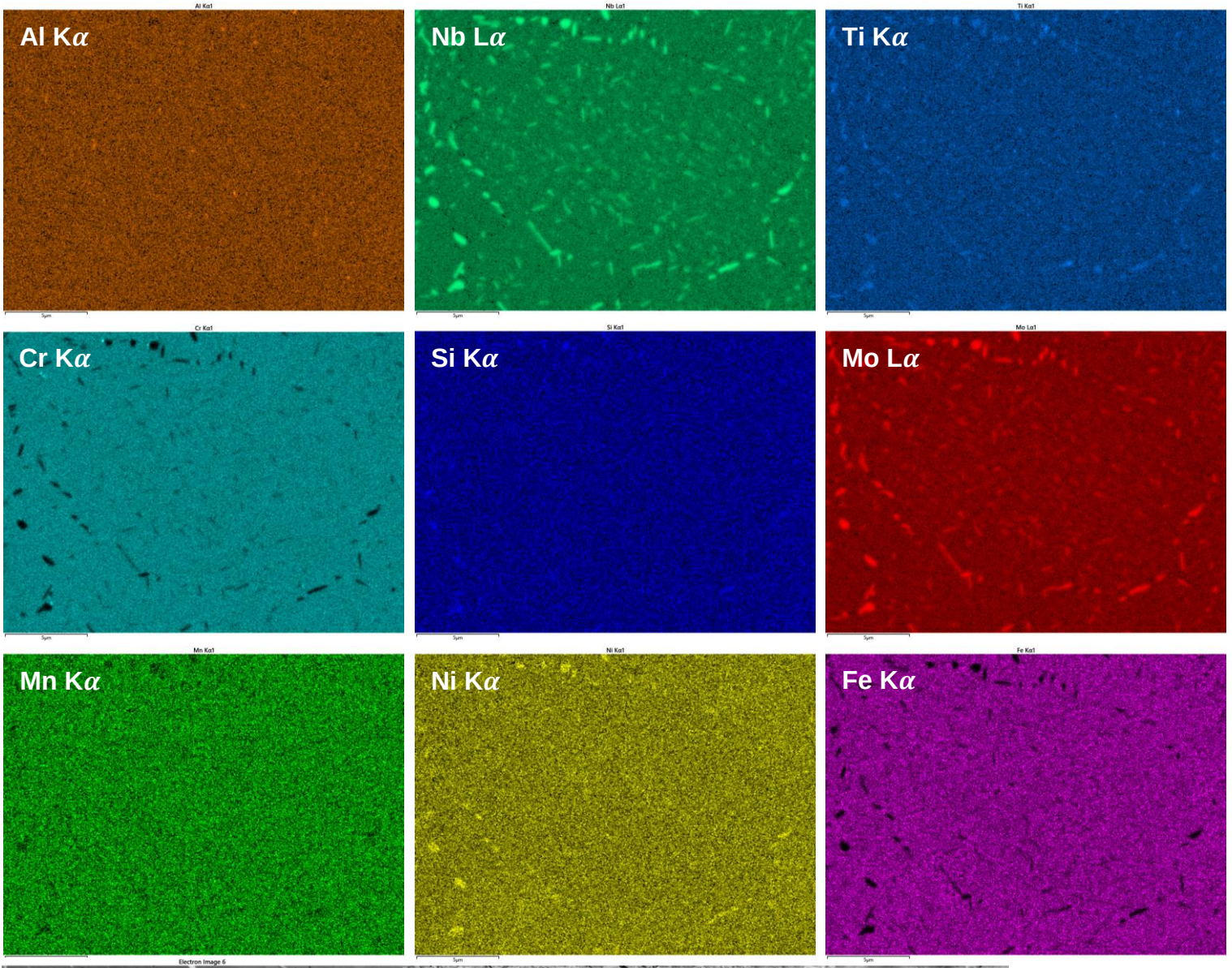

Figure 7. Maps for the IN718 AM+SA sample.

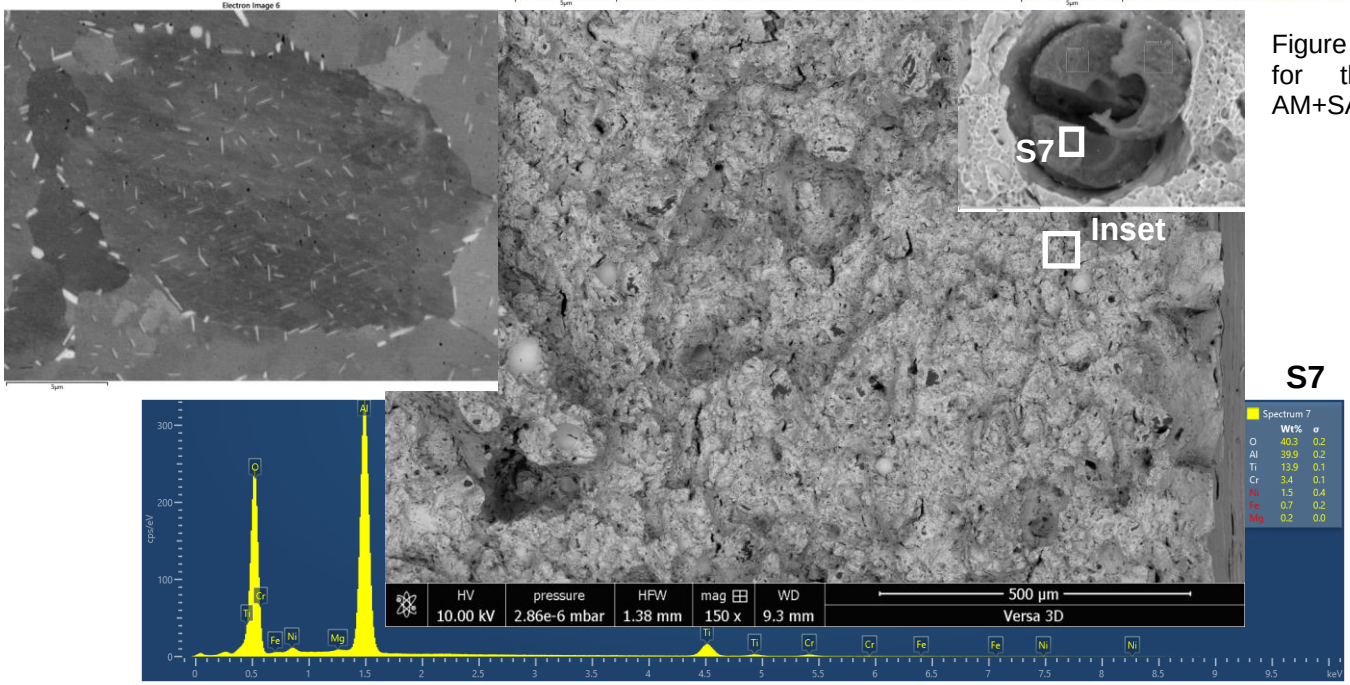

Figure 8. BSE micrographs and EDS analysis of the fracture surface from a room temperature Charpy impact specimen for an AM+SA IN718 sample showing transgranular fracture, inclusion from the inset and EDS analysis from the inclusion.

This indicates that those with globular and irregular morphology were carried over from powder and those with elliptically elongated morphology were formed in the melt pool during AM processing as suggested in Ref. [12] and as a result of increased oxygen levels from 0.0140 wt.% in the powder sample to 0.0270 wt.% in the AM+SA sample. Needle-like precipitates were observed to be Nb- and Mo-rich in AM IN625 after a heat treatment at 870^{o}C for 0.5-8 h [6] and Nb-, Mo- and Ti-rich in SLM IN718 followed by homogenisation or homogenisation and HIPing [15].

Despite the presence of Al-Ti oxide particles, precipitates and δ phase in AM+SA IN718, the fracture mode was predominantly transgranular ductile. An example of an Al-Ti oxide particle on a fracture surface is shown in Fig. 8 from a Charpy impact test of AM+SA IN718 at room temperature. The average value of Charpy impact tests was 20 J at room temperature.

Conclusions

Automated SEM/EDX has sampled an Al-rich foreign particle in gas-atomised IN718 powders (area fraction of 9.78 x 10^{-5}) showing the potential for cleanliness analysis. Thermally stable Al-Ti-(Mg) oxides were found both on the powder surface and intraparticle. Histograms of number density of inclusions in additive manufactured IN718 showed predominantly Al-Ti oxides. Despite the presence of Al-Ti oxide particles, precipitates and δ phase in AM+SA IN718, the fracture mode was found to be mainly transgranular ductile in Charpy impact testing at room temperature that had an average value of 20 J.

Acknowledgements

The financial support of Liberty Speciality Steels is gratefully acknowledged. This work was carried out as part of the UK government's Advanced Manufacturing Supply Chain Initiative (AMSCI) - CASCADE project.

References

[1] J.H. Martin, B.D. Yahata, J.M. Hundley, J.A. Mayer, T.A. Schaedler and T.M. Pollock: '3D printing of high-strength aluminium alloys', *Nature*, 2017, Vol. 549, pp. 365-369.

[2] E. Hryha, R. Shvab, H. Gruber, A. Leicht and L. Nyborg: 'Surface oxide state on metal powder and its changes during additive manufacturing: an overview', Proceedings Euro PM2017 (Milan; Italy; 1-5 October 2017).

[3] S.A.E. Aerospace, Aerospace Material Specification: AMS 5662, SAE International 2009.

[4] S.A.E. Aerospace, Aerospace Material Specification: AMS 5383, SAE International 2012.

[5] D. Zhang, W. Niu, X. Cao and Z. Liu: 'Effect of standard heat treatment on the microstructure and mechanical properties of selective laser melting manufactured Inconel 718 superalloy', *Mater. Sci. Eng. A* 2015, Vol. 644, 32-40.

[6] F. Zhang, L.E. Levine, A.J. Allen, M.R. Stoudt, G. Lindwall, E.A. Lass, M.E. Williams, Y. Idell and C.E. Campbell: 'Effect of heat treatment on the microstructural evolution of a nickel-based superalloy additive-manufactured by laser powder bed fusion', *Acta Materialia* 2018, Vol. 152, 200-214.

[7] Y.L. Kuo and K. Kakehi: Influence of powder surface contamination in the Ni-based superalloy alloy718 fabricated by selective laser melting and hot isostatic pressing', *Metals*, 2017, Vol. 7 (9), 367. https://doi:10.3390/met7090367

[8] E. Santecchia, P. Mengucci, A. Gatto, E. Bassoli, L. Denti, F. Bondioli and G. Barucca, Euro PM2018, Bilbao, Spain.

[9] C. Blackwell, S. Hall, J. Dawes and N. Brierley, Euro PM2018, Bilbao, Spain.

[10] C. Blackwell: 'Powder contamination analysis of In718 and 316L', MTC Report 2017.

[11] A.N.D. Gasper, B. Szost, X. Wang, D. Johns, S. Sharma, A.T. Clare and I.A. Ashcroft: 'Spatter and oxide formation in laser powder bed fusion of Inconel 718', *Additive manufacturing*, 2018, Vol. 24, 446-456.

[12] Y. Sun, R. Hebert and M. Aindow: 'Non-metallic inclusions in 17-4PH stainless steel parts produced by selective laser melting', *Materials and Design*, 2017, Vol. 140, 153-162.

[13] M. Nuspl, W. Wegscheider, J. Angeli, W. Posch and M. Mayr: 'Qualitative and quantitative determination of micro-inclusions by automated SEM/EDX analysis', *Anal. Bioanal. Chem.* 2004, Vol. 379, 640-645.

[14] Powder Diffraction File PDF-2 database, 2011, JCPDS-International Centre for Diffraction Data, Newtown Square, PA, USA.

[15] A. Mostafa, I. Picazo Rubio, V. Brailovski, M. Jahazi and M. Medraj: 'Structure, texture and phases in 3D printed IN718 alloy subjected to homogenization and HIP treatments', *Metals*, 2017, Vol. 7 (6), 196. https://doi.org/10.3390/met7060196.